ELSEVIER

Earth and Planetary Science Letters 168 (1999) 219–232

EPSL

Asian summer monsoon instability during the past 60,000 years: magnetic susceptibility and pedogenic evidence from the western Chinese Loess Plateau

Xiao-Min Fang [a,b,c,*], Yugo Ono [b], Hitoshi Fukusawa [c], Pan Bao-Tian [a], Ji-Jun Li [a], Guan Dong-Hong [a], Keiichi Oi [b], Sumiko Tsukamoto [c], Masayuki Torii [d], Toshiaki Mishima [e]

[a] *Department of Geography, Lanzhou University, Lanzhou, Gansu 730000, China*
[b] *Graduate School of Environmental Earth Science, Hokkaido University, Sapporo 060, Japan*
[c] *Department of Geography, Tokyo Metropolitan University, Hachioji 192-03, Japan*
[d] *Faculty of Informatics, Okayama University of Science, Okayama 700-0005, Japan*
[e] *Graduate School of Science and Technology, Kobe University, Kobe 657-8501, Japan*

Received 28 January 1999; revised version received 20 February 1999; accepted 20 February 1999

Abstract

The 28 m high-resolution Shajinping loess section in Lanzhou on the western Chinese Loess Plateau records a 60 ka, millennial summer monsoon variation. The record shows that Asian summer monsoons have rapid episodic pulse enhancements spanning only ca. 1–2 ka in high-frequency domain and having sub-Milankovitch cycles of progressive weakening in low frequency domain in the last glaciation. Soil formation seems to occur with a surprisingly fast response to these summer monsoon enhancements, resulting in weakly or moderately developed paleosol sequences. Both the pattern and timing of the summer monsoon enhancements show that they can be correlated to most major warm (Dansgaard–Oeschger) episodes and long-term cooling (Bond) cycles of the North Atlantic climatic records, indicating a possible teleconnection between tropic oceanic air masses and the North Atlantic climatic system. But differences exist for the transition of MIS 2/3 and the Holocene, where extraordinarily heavy dust-input events and fairly variable climatic fluctuations occur for the former and latter, respectively. A westerlies-swing model is proposed to interpret this link.

Keywords: monsoons; paleoclimatology; climate effects; magnetic susceptibility; loess; Paleosols; Loess Plateau

1. Introduction

Asian monsoons are a very important part of the global climatic system and consist mainly of summer and winter monsoons [1]. Summer's warm, moist air masses over the tropical Pacific (East Asian monsoon) and Indian (Indian monsoon) oceans bring heat and rain to East Asia [1] and develop soils. Cold masses of Siberian High air in winter generate dust storms and long-distance dust transport [2]. Continuous Chinese paleosol–loess sequences recorded the past 2.5 Ma of the Asian monsoon system variations [2,3]. The high correlation between Chinese loess–paleosol climatic and marine oxygen isotope (MIS) records further shows that summer monsoon varia-

* Corresponding author. +86-931-891-3362;
E-mail: fangxm@lzu.edu.cn

0012-821X/99/$ – see front matter
PII: S0012-821X(99)00053-9

tions closely follow low-frequency global climatic changes [2,3]. However, to provide information for predicting future climates and understanding the behavior and mechanism of global climatic changes, high-resolution records of summer monsoon changes are very necessary. This is somewhat strengthened by recent studies demonstrating that Asian winter monsoon may teleconnect to massive iceberg discharges into the North Atlantic Ocean (Heinrich events) [5–7] during the last extremely cold glacial episode [4]. Indian monsoon variations during the last glaciation may also have some teleconnection with episodic-large, sharp air- and sea-surface temperature fluctuations (Dansgaard–Oeschger events and Bond cycles) [6–9] in the North Atlantic region [10,11]. To achieve the goals above, especially to clarify the possible teleconnections between Asian monsoons and the North Atlantic climate, we present a 60,000 year century-scale summer monsoon record from the western Chinese Loess Plateau.

The western Chinese Loess Plateau is nearest to the source area of aeolian dust. It has about a three to four times higher dust deposition rate than the central Loess Plateau. Consequently, it has the world's thickest loess (318 m) deposit. In the Lanzhou area the deposit covers a relatively short geological time (only 1.3 Ma) [12–14]. A further advantage of the Lanzhou area is that it is located in the northwestern front of summer monsoon circulation and so has a strong gradient between warm-humid air masses over the Pacific–Indian Ocean and cold-dry air masses centered over the Siberian–West Mongolian areas [2,3]. Lanzhou receives much less precipitation and has weaker pedogenesis than the central Loess Plateau [15,16]. Consequently, loess deposits in the Lanzhou area have a great potential for revealing detailed monsoon history and detecting both winter and summer monsoon signals with much higher resolution than in the central Loess Plateau. In fact, the last interglacial and mega-interstadial paleosols (S1 and Sm series) developed as three or more individual soils separated by intervening loess. Their total thickness reaches at least ca. 8–10 m [12–14] (Figs. 1 and 2), while S1 and Sm in the central Loess Plateau have a thickness of only ca. 2–3 m and occur as a single polygenetic soil [2,3]. Thus, we chose the Lanzhou loess at Shajinping to make a detailed study of summer monsoon history during the past 60,000 years, based on multi-proxy evidences such as pedogenesis, magnetic susceptibility, carbonate content and soil color.

2. Stratigraphy, sampling and laboratory work

The Shajinping loess section is in Lanzhou City on the north side of the second terrace of the Huang He (Yellow River) Valley (36ºN and 103º50′E; Fig. 1). The section is in a very fresh outcrop cut in 1995 for a rail station. The section is ca. 28 m thick and represents the uppermost part of the Lanzhou loess. It covers the alluvial loess and terrace gravels of Huang He (Fig. 1) [14]. It consists of 2.45 m Holocene loess with one embedded, moderately developed S0 series paleosol at the top, 19.75 m of aeolian Malan (L1) Loess of the last glacial in the middle, and about 5 m alluvial silts at the bottom (Fig. 2). We identified eighteen weakly to moderately developed paleosols in the Malan Loess. We correlated three of the paleosols (L1S1–L1S3) with the last glacial (MIS 2) and fifteen (L1S4–L1S18) with the last mega-interstadial (MIS 3) (see below for details on the correlation and dating). Typical and weathered loesses (L1L1 to L1L19) occur between these paleosols (Fig. 2). The paleosols can be further grouped into eight soil complexes (GS1 to GS8). Each group generally begins with a relatively strong or thick paleosol and is followed by a weak thin paleosol or weathered loess separated by thick unweathered loess. The lowermost four soil complex groups (GS5 to GS8) can be correlated with the previous low-resolution, last mega-interstadial Sm soil series (Sm-1 to Sm-3/Sm-4) [13] (Fig. 2). The real top of the section was cut away to make a flat field for farming, which could explain the small thickness of the Holocene loess, the absence of other Holocene soils in our section (the normal Holocene loess is ca. 4 m thick and S0 consists mainly of three to four individual soils in Lanzhou [13,14]), and the relatively lower magnetic susceptibility of the Holocene.

Field observations and laboratory analyses have indicated that the moderately developed paleosols are Luvic Calcisols [17]. A brief description follows:

(1) Ah — very thin ochric horizon, gradual boundary to the loess above and the Bw horizon below;

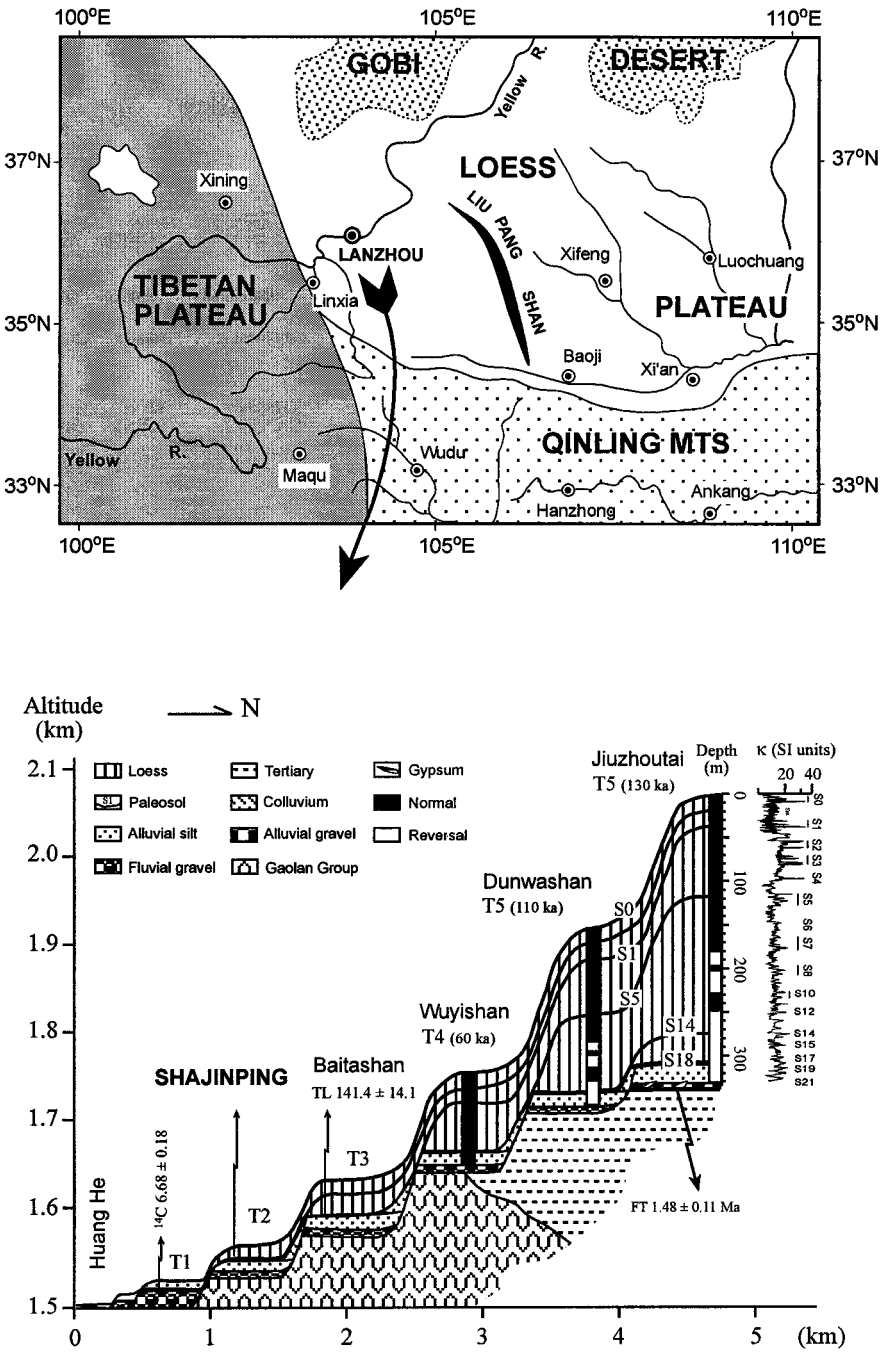

Fig. 1. Locality map and typical loess–paleosol sequence in the Lanzhou region. Note that the loess–paleosol sequence is continuously distributed on terraces of Huang He in Lanzhou and confirmed by intensified multiple-approach dating of the sequence and terraces by Burbank and Li [12] and Li et al. [14] (modified from reference [14]). Note the 318 m world's thickest loess deposit with 18 embedded paleosols identified by pedogenesis and magnetic susceptibility (κ) at Jiuzhoutai on the seventh terrace T7.

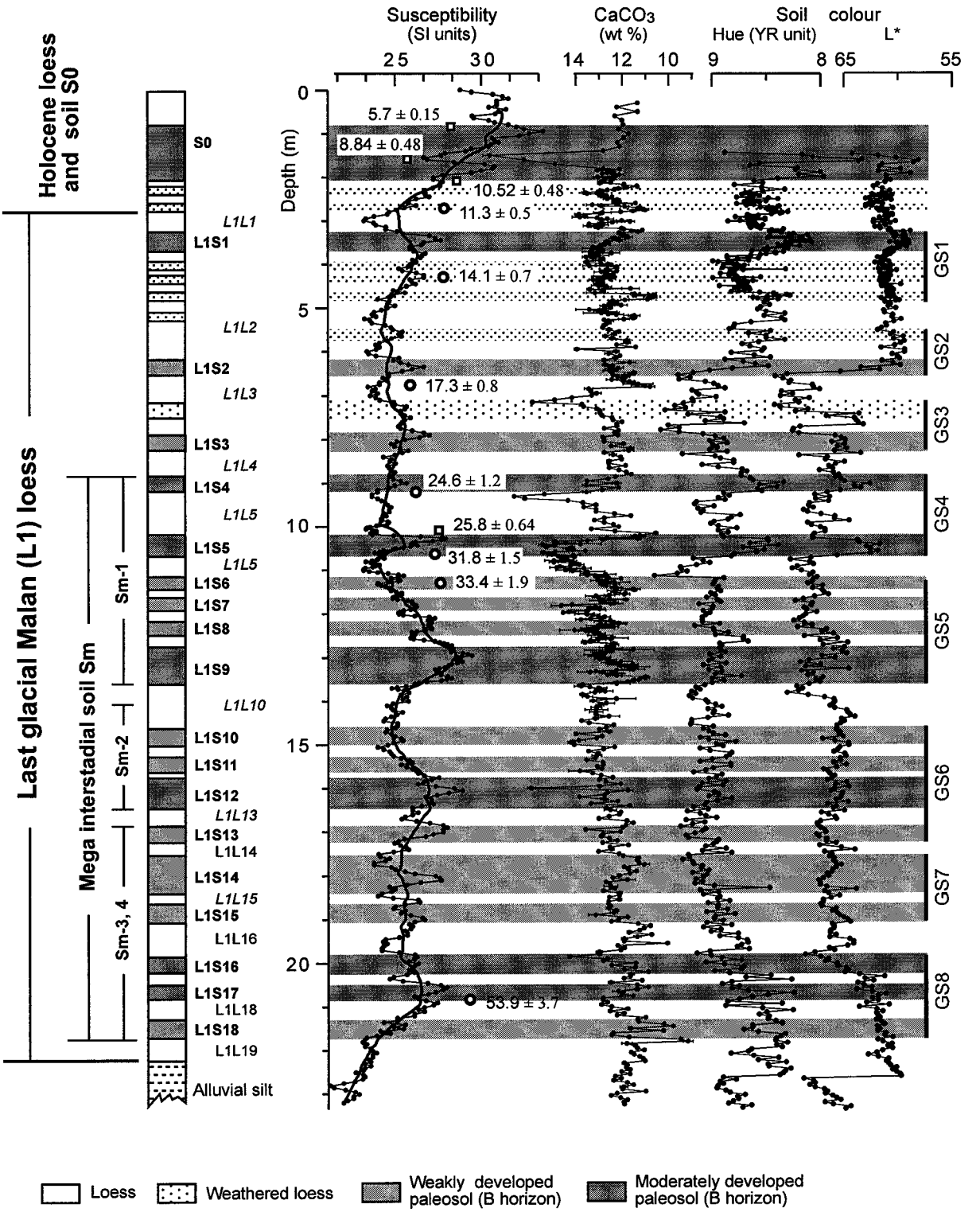
Susceptibility (SI units)
25 30
CaCO3 (wt %)
14 12 10
Soil colour
Hue (YR unit)
9 8
L*
65 55
Depth (m)
0
5
10
15
20
5.7 ± 0.15
8.84 ± 0.48
10.52 ± 0.48
11.3 ± 0.5
14.1 ± 0.7
17.3 ± 0.8
24.6 ± 1.2
25.8 ± 0.64
31.8 ± 1.5
33.4 ± 1.9
53.9 ± 3.7
Holocene loess and soil S0
Last glacial Malan (L1) loess
Mega interstadial soil Sm
Sm-1
Sm-2
Sm-3, 4
S0
L1L1
L1S1
L1L2
L1S2
L1L3
L1S3
L1L4
L1S4
L1L5
L1S5
L1L5
L1S6
L1S7
L1S8
L1S9
L1L10
L1S10
L1S11
L1S12
L1L13
L1S13
L1L14
L1S14
L1L15
L1S15
L1L16
L1S16
L1S17
L1L18
L1S18
L1L19
Alluvial silt
GS1
GS2
GS3
GS4
GS5
GS6
GS7
GS8
Loess
Weathered loess
Weakly developed paleosol (B horizon)
Moderately developed paleosol (B horizon)

(2) Bw — a 50 cm or so thick cambic horizon, relatively distinct dull brown (7.5YR 5/3–7.5YR 6/4 by Munsell color charts), loam or silt loam, medium angular blocky structure, relatively rich in organic matter (2–4 wt %) and clay (ca. 8–10 wt %), low in carbonate, ca. 10 wt %, with common biological channels (ca. 5–10 area %) and excrements (ca. 5 area %);

(3) Bk — a 10–20 cm thick calcic horizon, massive, with up to 16 wt % of carbonates as fine nodules, channel coatings and infillings;

(4) C — light yellowish brown (10YR 7/2-3) loess, silt loam, massive, ca. 13 wt % carbonate occurring mainly as coarse primary grains, low amounts of organic matter, biological pedofeatures (channels and excrements less than 3 area %, respectively) and clay (<5 wt %).

Most of the weakly developed paleosols have a 20–30 cm thick dull yellowish brown (10YR 5/4–10YR 4/3 when dry) silt loam ochric or mollic horizon (sometimes with thin AB horizon below), with massive to medium blocky structure, slight accumulations of organic matter, low clay (ca. 5 wt %) and carbonate contents (ca. 11 wt %) as fine nodules and thin coatings.

Weathered loess is intermediate in development between weakly developed soil and typical loess. The alluvial silt has very distinct laminations. Paleosols below a depth of 18 m have involution-like microfolds and some undulating thin horizons possibly resulting from freeze–thaw or alluvial processes.

Samples were taken at 2–5 cm intervals for carbonate content and rock magnetism. A total of 672 samples were collected, yielding a resolution of about 40–100 years per sample. Magnetic susceptibility (κ) was measured in the field at 5 cm intervals for most of the section and at 2.5 cm intervals for important stratigraphic intervals using a Bartington MS2 susceptibility meter.

Carbonate content was analyzed with a standard Bascomb calcimeter [18]. The data are means of two to four analyses per sample. The average standard deviation was 0.16 wt % of carbonate. Color of a dried powdered sample was measured on a white plate with a Minolta CM508i color meter. This meter measures the reflected laser light from the sample.

3. Chronology

Previously, systematic, multiple-approach dating of loess stratigraphy on all terraces of Huang He demonstrated that the soil sequence in the Lanzhou region is fairly stable (Fig. 1). Paleosols S0 and Sm have ages of ca. 2–10 ^{14}C ka and ca. 23–55 ka, respectively, and can be well correlated with warm periods of marine isotope records MIS 1 and 3, respectively [12–14,16,19] (Fig. 1). The continuity of paleosol Sm on terrace T2 and higher ones (Fig. 1) indicates that T2 was formed immediately before Sm at ca. 55 ka [13,14]. This age is in good agreement with ages of all T2 terraces studied in the middle and upper reaches of Huang He [20,21]. This pedostratigraphic control also is strongly supported by the SPECMAP stack [22] and by the great resemblance of the smoothed magnetic susceptibility curve from the Shajinping section to the low-resolution magnetic susceptibility curves of paleosols S0 and Sm from other sections in Lanzhou (Figs. 1 and 2) [13,14]. These facts provide framework constraints for the chronology of the Shajinping section.

Detailed chronology of the section is constrained by eleven ages obtained from bulk organic radiocarbon and infrared stimulated luminescence (IRSL) dating [23] (Table 1; Fig. 3). All ^{14}C ages had been determined with a half-life of 5730 years by the Geography Department of Lanzhou University. We converted these apparent ^{14}C dates into the calendar year. First we corrected the ^{14}C dates for a half-life of 5568 years and a δ^{13}C value of 18.3‰ (mean of paleosol S0 on the Loess Plateau [24]). For ^{14}C ages younger than 18,360 yr B.P. we applied a tree ring

Fig. 2. Stratigraphy and magnetic susceptibility and carbonate content curves of the Shajinping loess section, Lanzhou. Paleosols were identified independently in the field. Heavy line indicates 21-point moving average of susceptibilities. 1σ errors are plotted for carbonate curve as horizontal bars. Color data are taken from Fukusawa and Koizumi [11]. Italics indicate thick loess layers separating grouped soils. Square indicates radial carbon data from Li et al. [13] for the corresponding sequence in the nearby Jiuzhoutai loess section (see Fig. 1) and circle marks IRSL data from Tsukamoto [23].

Table 1
Chronological constraints for the Shajinping loess section

Depth (cm)	Sequence	^{14}C age (ka BP)	Calendar age (ka BP)	Method or dataset used for calibration
90	Top of S0	4.99 ± 0.1	5.70 ± 0.15 [a,c]	Tree ring chronology [25]
170	Lower of S0	8.10 ± 0.31	8.84 ± 0.48 [a]	Tree ring chronology [25]
200	Bottom of S0	9.65 ± 0.37	10.52 ± 0.48 [a]	Tree ring chronology [25]
260	Middle of L1L1		11.3 ± 0.5 [b]	IRSL [23]
415	Middle of L1L2		14.1 ± 0.7 [b]	IRSL [23]
680	Middle of L1L3		17.3 ± 0.8 [b]	IRSL [23]
910	Top of L1L5		24.6 ± 1.2 [b]	IRSL [23]
1025	Top of L1S4	22.49 ± 0.64	25.8 ± >0.64 [a,c]	U–Th vs. ^{14}C age dataset [26,27]
1035	Middle of L1S5		31.8 ± 1.5 [b]	IRSL [23]
1105	Bottom of L1L5		33.4 ± 1.9 [b]	IRSL [23]
1700	Middle of L1S13		45.5 ± 0.53 [b]	Correlation to GRIP ice core [8]
2060	Top of L1S17		53.9 ± 3.7 [b]	IRSL [23]
2165	Bottom of L1S18		56.3 ± 0.53	Correlation to GRIP ice core [8]

[a] Calibrated ^{14}C age.
[b] Infrared stimulated luminescence age.
[c] Ages based on correlation.

calibration from a combined dataset [25] using the CALIB 3.0 ^{14}C age calibration program [25]. For ^{14}C ages older than 18,360 yr B.P. we used a ^{14}C age–U/Th age calibration based on paired analyses given in Bard et al. [26,27] (Table 1). These analyses have errors of less than 500 years.

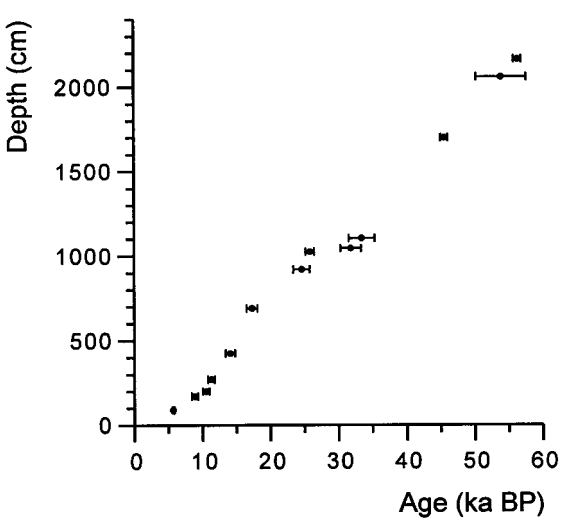

Fig. 3. Age–depth relationship of the Shajinping loess section (data are taken from Table 1; horizontal bar indicates 1σ error of date). The large slope between about 24 ka and 12 ka BP marks a striking increase in loess accumulation rate from MIS 3 to MIS 2.

Taking into account the scarcity of dates and the large errors with the last two IRSL dates from the middle and lower parts of the section, two additional age constraints were assigned from the δ^{18}O curve of GRIP ice core [8] to summer monsoon enhancement event 12 at depth of 1700 cm and stage boundary of MIS 3/4 identified in the magnetic susceptibility record (Table 1). Uncertainties with these correlations (caused by a gradual transition of soil–loess boundaries mostly within 10–20 cm) are about 270–530 years, if an averaged loess depositional rate of 37.65 cm/ka is considered for the section.

To refine the chronology, we employed a grain size–age model [4] to calculate ages for all sampling stratigraphic levels between the age constraints (except some biased ones from the fitted curve of age–depth pairs). The model works on the assumption that the coarse size fraction is proportional to the dust accumulation rate and thus wind strength. That is that enhancing the winter monsoon (wind strength) will cause a linear increase of the dust input rate and content of the coarse size fraction. This method benefits linear interpretation between age constraints because winter monsoon and loess deposition rates changed sharply in the past [2–4]. Thus, the resolution and the dating of the section enables a fairly detailed comparison of loess–paleosol proxies and ice cores within their error ranges (Table 2).

Table 2
Ages of large magnetic susceptibility peaks for the Shajinping section derived by alternative dating methods

Peak No.	Stratigraphic depth susceptibility maximum (cm)	^{14}C and IRSL [a] (ka BP)	Linear interpolation [b] (ka BP)	Grain size model [c] (ka BP)	Oxygen isotope peak in GRIP ice core [c] (ka BP)
1	345 (322–440) [e]	12.8 (12.4–14.4)	13.6 (13.2–15.7)	12.9 (12.4–14.6)	14.3 (12.6–14.7)
2	795 (715–805)	21.2 (20.5–22.4)	21.2 (20.5–21.6)	22.4 (20.7–22.5)	21.3 (20.6–21.7)
4	1035 (972–1050)	26.1 (25.8–26.4)	25.9 (24.1–26.3)	26.1 (25.8–26.5)	25.9 (25.7–26.4)
7	1215 (1207–1243)	30.7 (30.4–31.4)	30.9 (30.7–31.7)	30.0 (29.9–30.7)	31.7 (31.3–32.2)
8	1302 (1278–1365)	32.9 (32.3–34.5)	33.3 (32.7–35.1)	32.2 (31.5–33.9)	34.5 (32.8–35.0)
12	1700 (1680–1732)	43.0 (42.5–44.0)	44.4 (43.9–45.3)	43.0 (42.6–43.9)	43.0 (41.5–43.3)
13	1810 (1792–1830)	46.3 (45.8–46.9)	47.5 (47.0–48.1)	46.2 (45.7–46.8)	45.5 (44.9–45.6)
14	1905 (1858–1945)	49.2 (47.8–50.4)	50.2 (48.9–51.3)	49.1 (47.5–50.3)	50.9 (48.3–50.0)
15	2010 (1993–2032)	52.4 (51.9–53.1)	53.1 (52.6–53.7)	52.1 (51.6–53.1)	52.3 (52.2–52.6)
16	2060 (2048–2123)	53.9 (53.5–55.3)	54.5 (54.2–56.3)	53.9 (53.6–55.3)	54.7 (53.9–55.1)
17	2150 (2147–2165)	56.1 (56.0–56.3)	57.0 (56.9–57.4)	55.9 (55.8–56.3)	55.9 (55.4–56.3)

[a] Linear interpolation between ages from ^{14}C and IRSL determinations.
[b] Linear interpolation between MIS 1/2, 2/3 and 3/4 boundaries [22] (approximately corresponding to the bottom of paleosol S0 and the bottom and top of paleosol Sm series, respectively).
[c] Grain size model [4] applied between age constraints.
[d] Ages of δ^{18}O minima are taken from reference [8].
[e] Position of maximum value in a peak and the peak range (in parentheses).

4. Summer monsoon proxy

Soil magnetic susceptibility is chiefly a function of type, concentration and grain size of soil magnetic minerals, if the contributions of paramagnetic and diamagnetic mineral susceptibilities and susceptibility anisotropy are small. It has been widely demonstrated that enhancement of magnetic susceptibility in soil is mainly caused by enrichment of superparamagnetic (SP) or ultrafine (<0.03 μm for magnetite [28]) magnetic grains through soil formation [28–31]. Magnetic susceptibility, therefore, is widely used as a sensitive indicator of Asian summer monsoons [2,3]. In the Shajinping section, detailed rock magnetic study has shown that there is no significant change in magnetic mineral composition [32]. Magnetic susceptibilities at Shajinping then may directly reveal pedogenic and climatic signals.

Carbonates in Lanzhou loess are composed mainly of fine sand- and coarse silt-size calcite and lesser amounts of dolomite distributed throughout the groundmass [15,16]. In the western Loess Plateau amounts of carbonate are ca. 12 wt % and ca. 9 wt % in the central Loess Plateau [2,13,15], suggesting fairly mixed airborne dusts before deposition. This suggestion is supported by a large body of other evidence [2]. Soil micromorphology has further shown that primary carbonate grains in loess on the western Loess Plateau have changed little, while those in paleosols have clearly undergone a size reduction to an average of ca. 5 μm and are precipitated in lower Bk horizon as secondary calcite pedofeatures such as coatings and nodules [15,16]. This may suggest that soil genesis is the main factor responsible for large carbonate fluctuations between loess and paleosol, in which precipitation is the major direct driver. This is to be expected because carbonate is more sensitive to precipitation than to temperature. Nearly a linear relationship between modern soil carbonate content and leaching depth and precipitation is commonly found over China and other continental subhumid–arid areas [33,34]. A case study from Africa shows that leaking from an irrigation system caused a nearly complete leaching of carbonates in underlying soils over a decade of years or more [35]. In monsoonal Asia, high precipitation is generally accompanied with high temperature [1], facilitating leaching of carbonates in soil and loess. High correlations of carbonate, magnetic susceptibility, and deep-sea records in low- and high-frequency domains [4,15] demonstrate their practicability in

revealing climatic changes both in orbital and millennial scales.

Soil color has long been the best-known soil property. It is an important diagnostic property for soil classification or composition study, because it is a function of composition of soil primary and secondary minerals and organic matter [33]. In general, soil color has been demonstrated to have a good relationship with temperature and precipitation in humid to semi-arid areas, but a somewhat arbitrary relationship in arid areas [34].

Soil color can be described either in a Munsell color system as functions of hue (representing the dominant spectral like red, yellow, green, blue, etc.), value (representing the relative lightness of color) and chroma (representing the relative purity or strength of the spectral color), or in a L^*–a^*–b^* color system as values of parameters L^* (varying between white at 100 and black at 0), a^* (varying between red and green) and b^* (varying between yellow and blue). Therefore, hue can be generally used as a first-order indicator to identify different types (thus environments) of soils or to separate soils from their parent materials. Hue strongly reflects the soil redness contributed principally by iron oxides, hydroxides and iron-rich clay minerals [34–37], which are also the chief minerals contributing to magnetic susceptibility. For loess and paleosols on the western Loess Plateau, hue varies mostly between 7.5YR (paleosols) and 10YR (loesses). In monsoonal China soil redness increases with increase in content of iron oxides and hydroxides and with increase in temperature and precipitation [34]. This is not only true for luvic and lateritic soils in warm-humid East and South China, but also true for cambic and calcic soils in cool-humid and semi-arid North and West China [33,34]. For soils in very arid or cold humid areas, hue seems to change arbitrarily, probably due to very weak weathering or for variation in iron oxide content of the parent materials. The study site is located in a semi-arid zone. Thus, hue is chosen as a proxy of pedogenic type and degree of weathering for this study.

Obviously, soil organic matter and carbonates should have a great deal of influence on value or L^* of soil color. Nagajima has shown a clear negative proportion of L^* to organic matter that records mainly vegetative change linked to climatic conditions [37]. Because L^*, in concept, has a clearer measure of white and black colors than has value, thus a higher sensitivity to degree of organic matter and carbonates, we use L^* in this study to reconstruct bioclimatic history.

A successful example of utilization of hue and L^* in revealing climatic change comes from an intensive study of 2.5 Ma Luochuan type loess section on the central Loess Plateau. That study shows that hue and L^* correlate ($r > 0.8$–0.9) with the magnetic susceptibility of the section [38] and encourages the exploration of soil color for this study.

Other attributes or parameters of soil color are not used in this study due to uncertainty of clear links with climatic conditions other than soil environmental processes such as oxidation-reduction.

We, therefore, use magnetic susceptibility as a major direct analog of summer monsoon, carbonate content as an indicator of precipitation, and soil hue and L^* as supporting summer monsoon signals, and direct signals of pedogenesis. In practice, only the peaks which indicate a remarkable change of magnetic susceptibility, carbonate content (leaching in Bw horizon and accumulating in Bk horizon), and soil color are regarded as major enhancements of Asian summer monsoons.

5. Summer monsoon changes over the last 60,000 years

In the Shajinping section magnetic susceptibility, carbonate, and color time series have a general similarity in millennial variation. All three suggest high-frequency and large-amplitude summer monsoon changes in the last glacial. The pattern has seventeen identical warm peaks or summer monsoon enhancements SME1 to SME17, each one spanning a time interval of ca. 1–2 ka and corresponding to one of the paleosols (Table 2; Figs. 2 and 4). Furthermore, the seventeen warm peaks can be grouped into eight peaks (GP1 to GP8), which correspond roughly to the GS1 to GS8 soils (Figs. 2 and 4). Each grouped peak, starts with a higher warm peak corresponding to a moderately developed soil or a thick soil and ends with a progressively lower peak corresponding to a weakly developed soil or weathered loess. The time span for each is about 6–8 ka and is separated

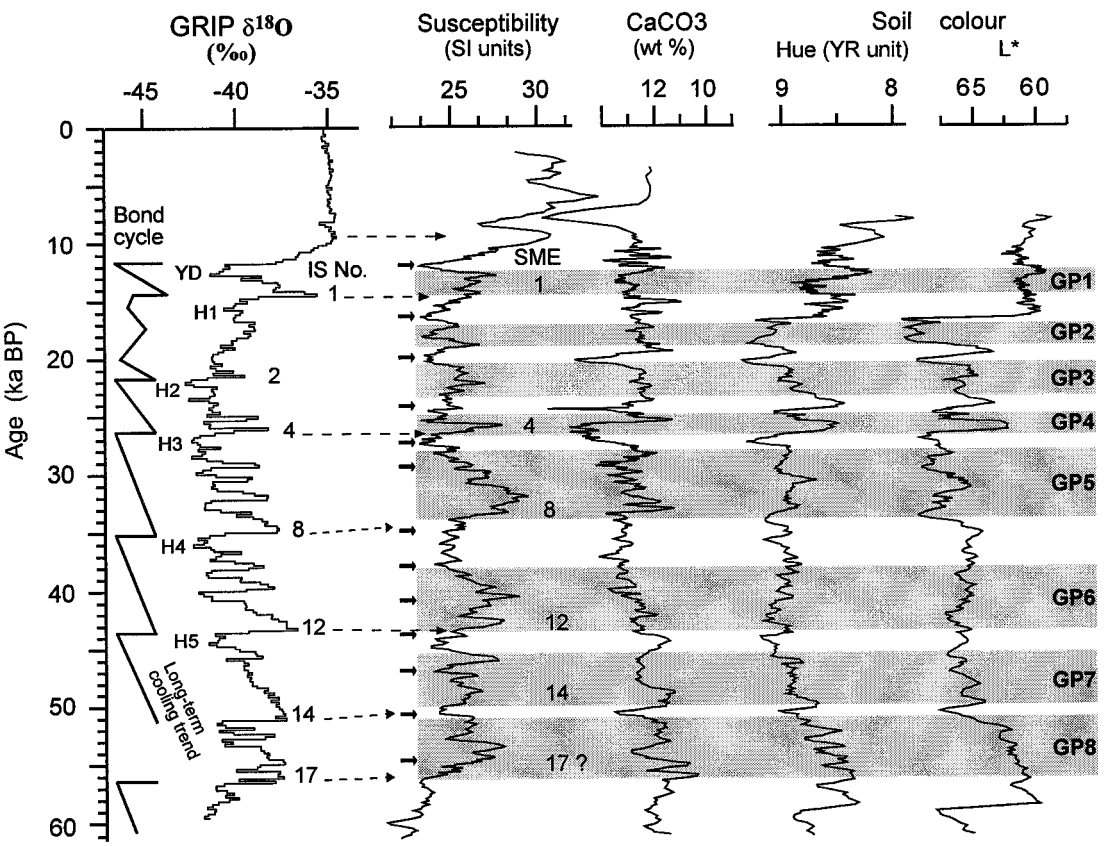

Fig. 4. Correlation of major summer monsoon enhancements (*SME*) and their grouped peaks (*GP*) suggested by 3-pt moving averages of magnetic susceptibility, carbonate and color time series based on Table 1 from the Shajinping section with isotope warm peaks (*IS No.*) of the Greenland GRIP ice core [8] and with Bond cycles [9]. Heavy arrows mark major coarse size fraction increases that may correlate with very cold intervals in the North Atlantic region. Placement of Bond cycles and Heinrich events (*H*) in the GRIP record was taken from Bond et al. [9].

by a large cold interval. A susceptibility minimum and hue minimum and a carbonate maximum and L^* maximum separate each group (Table 2; Fig. 4). The marked susceptibility and color minima or carbonate and L^* maxima, on the other hand, correspond to distinct thick loess layers (Figs. 2 and 4). Grain size analysis confirms that nearly all the major coarse size fraction peaks occur in the strongest winter monsoons [4]. They are in the thick loess layers and near the uppermost boundary of the paleosols and are followed by a progressive upward decrease in the coarse fraction ratio. This suggests that both summer and winter monsoons have fast enhancement and progressively weakening characteristics in low-frequency domain and short-large fluctuations in high-frequency domain (Fig. 4).

In the last glaciation both the pattern and chronology of the summer monsoon variations have a great resemblance to surface temperature changes derived from the oxygen isotope record of the Greenland GRIP ice core [8] and from *Neogloboquadrina pachyderma* (s.) in North Atlantic core V23-81 [9] (Fig. 4). Particularly, major identical summer monsoon peaks and their grouped ones from GP1 to GP6 in the four time series of magnetic susceptibility, carbonate, hue and L^* match with the main warm periods of the GRIP ice core (Dansgaard–Oeschger events) and the long-term cooling (Bond) cycles in core V23-81, respectively, within their error ranges (ca. 1–4 ka for older ages in the latter two cores) (Table 2; Fig. 4). This indicates that North Atlantic climate changes may affect not only summer mon-

soons and soil formation but also biological activity (vegetation and soil animals). However, the correlation for the lowest part of the section, especially below 18 m depth, can only be tentatively made on the scale of grouped peaks. It is very difficult on individual peaks, because the lower part of the Shajinping section seems to have been affected by alluvial processes (Fig. 4). This is perhaps why there are persistent lower values of carbonate, hue and L^* (caused by mottles due to oxidation-reduction) for the lowermost part of the section that has the loess L1L19 and alluvial silt. Differences between magnetic susceptibility, carbonate and color for the interval of about 40–45 ka are evident where increases of magnetic susceptibility are not accompanied by corresponding lower values of carbonate and color (Fig. 4). These differences may suggest that a summer monsoon enhancement did not accompany a corresponding increase in precipitation (thus less carbonate leaching) and strengthening of color-indicated pedogenic degree and biological activity, or summer monsoon was enhanced not strong enough to drive significant rains to the Lanzhou region to increase soil weathering and vegetation growth.

Detailed comparison between our record and North Atlantic climatic records [8,9] reveals two characteristic phenomena. One is that Holocene monsoonal Asia has a much larger climatic change than the North Atlantic and Greenland (Fig. 4), even there is some evidence showing that North Atlantic climatic fluctuations are larger than previously thought [39]. A large body of evidence from China confirms that the Asian Holocene experienced larger climatic fluctuations with more marked warming intervals centered at ca. 9.4, 6.3 and 2.5 ka than occurred in the high latitudes [40]. The other is that the large dust input rate increase is found in the transition from the warm period of stage 3 to the cold period of stage 2 within the last glacial maximum (Figs. 1 and 3).

6. Discussion

High-frequency and large-amplitude fluctuations of the North Atlantic climate [5,8,9] directly affect neighboring areas [6,41–43]. Porter and An [4] suggested that the extremely cold intervals at the ends of Bond cycles [9] affected Asian winter monsoon variations as indicated by grain size change in a Chinese loess–paleosol sequence on the central Loess Plateau.

Our record demonstrates that the summer monsoon appears to have been affected not only by the extreme but also other cold climates of Dansgaard–Oeschger events in the North Atlantic region [8]. Marine records from the South China and Japan Seas and the Indian Ocean have shown evident monsoon weakening during the Younger Dryas and Heinrich H1 events [10]. However, the $\delta^{18}O$ of planktonic foraminifera *Globigerinoides ruber* at the Sulu Sea Site 769 and foraminifera transfer function from the western tropic Pacific demonstrate that the western Pacific warm pool experienced no significant sea surface temperature change during the last glacial cycle (less than 2ºC from the present) [44,45]. Since the western Pacific warm pool is the major source supplying heat and moisture to the East Asian monsoon [1], the large fluctuations of the summer monsoon revealed from the Lanzhou loess–paleosol sequence during the last glacial could not be explained by the change of the western Pacific warm pool. Thus, changes in continental surface and air conditions, and thus in atmospheric circulation, would be the most likely involved mechanism.

It has been widely known that the Tibet Plateau has played a key role in adjusting Asian and Northern Hemispheric atmospheric circulation [14,46–48]. Theoretical thinking and numerical general circulation (GCM) modeling demonstrate that uplift of the Tibet Plateau in the late Cenozoic not only generated the Tibet Plateau monsoon — strong surface low pressure (Tibet Low) in summer and high pressure (Tibet High) in winter [46,49] — but also intensified the Northern Hemispheric temperature gradient through absorbing CO_2 enhanced by weathering processes [47], thus cooling global temperature, and strengthening the westerlies which act as a wall to hinder heat exchange between the Equator and high latitudes [48,49]. The Tibet Low is a major force attracting the burst and northwesterly flowing of the Indian monsoon, whereas the Tibet High enhances the strength of the westerlies and winter monsoon [48,49]. When the Tibet Plateau rose to a critical height, the overflowing westerlies was forced to diverge at the western margin of the plateau, thus

strengthening the flows and causing further a temperature drop [14,46–48].

This setting has basically determined the controlling roles of the Tibet Low and the westerlies on the summer monsoon. GCM modeling and meteorological data demonstrate that changes in the Tibet Low considerably changes the strength of the summer monsoon, and that changes in position and strength of the westerlies also greatly affect the summer monsoon [46–48]. Snow cover on the plateau and strength of the westerlies directly affect the Tibet Low and position of the westerlies in the Tibet region. Modern meteorological data show that an over-year snow cover or an increase of snow area in winter on the plateau results in a higher Tibet High in winter, but a lower Tibet Low and a weaker summer monsoon the following summer [46]. The westerlies move southwards and diverge into northern and southern jets during the winter half year, or even mostly stay in the southern margin of the plateau at times when an extremely cold polar intrudes southwards [1,46], leading to a great recession of the summer monsoon. Generally, the summer monsoon bursts in May with the shift of the southern jet of the westerlies to the north of the plateau, and progressively retreats during fall and winter [1].

Thus, we propose a westerlies-swinging model to explain our observations as follows. During high-insolation periods (interglacials or mega-interstadials), the Tibet Low may remain strong, possibly because of little or no snow cover and absorption of more insolation than other areas at the same latitude because of height. The westerlies may stay north of the Tibet Plateau the whole summer, causing a strong enhancement of the summer monsoon (Fig. 5a) and stronger pedogenesis. In contrast the decreased temperature of low-insolation periods (glacials or stadials) favors persistence of over-year snow cover on the plateau, thus reducing the Tibet Low and the summer monsoon, but enhancing the Tibet High and the strength and southward moving of the westerlies. This feedback enlarges snow cover on the plateau, thus further reducing the Tibet Low and enhancing the Tibet High and the westerlies. A repeating feedback causes a progressive retreat of the summer monsoon and a gradual intensification and southward moving of the westerlies (Fig. 5b). Any similar outside forcing like Bond cooling cycles of the At-

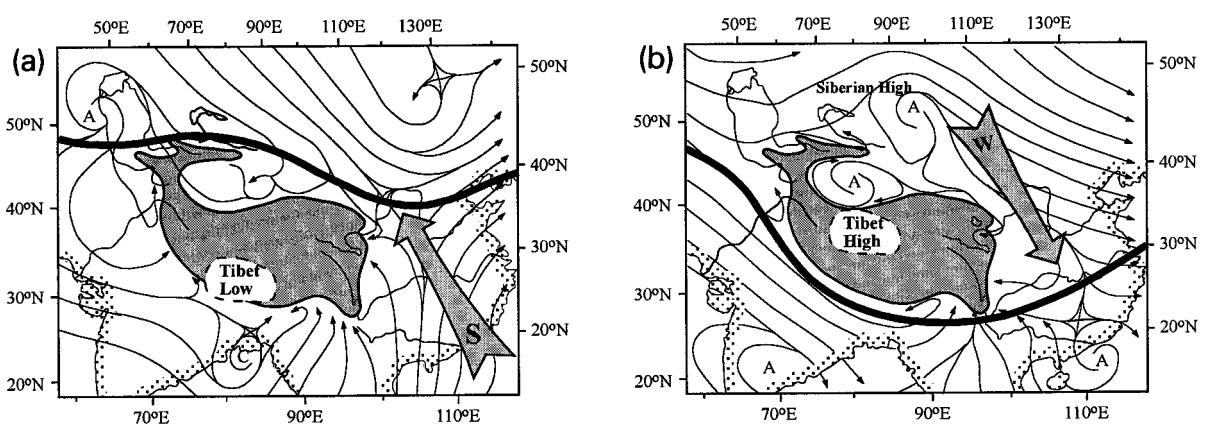

Fig. 5. Air circulation model based on construction of mean streamlines at the 1500 m level in July (a) and January (b) (1961–1970) for stronger summer monsoon enhancements in interglacials and mega-interstadials (a) and summer monsoon weakening (b). Heavy solid line indicates roughly the westerlies jet in strong summer monsoon enhancements (a) and full weakening (b). *A* and *C* are anticyclone and cyclone, respectively. Shaded arrows mark main directions of summer monsoon (*S*) and winter monsoon (*W*). Heavily shaded area indicates the 3000 m configuration of the Tibet Plateau. The mean positions of the Tibet Low in summer and High in winter shown on higher-level meteorological charts [46] are roughly plotted as broken line zones. Note that the streamlines in July indicate a clear shift of the westerlies to the north of the Tibet Plateau with strong outflow of oceanic moist air masses into Asian inland (a), a pattern working similarly for summer monsoon enhancements in interglacials and interstadials. Streamlines in January show a distinct divergence of the westerlies as south and north branches (b), a pattern probably for weak summer monsoon enhancements in smaller interstadials such as those in MIS 2. At times of full glacials or very cold stadials, the westerlies jet may shift completely to the south of the Tibet Plateau as indicated by the heavy solid line in (b). See text for details.

lantic climate causes a similar change of the summer monsoon. A similar pattern was suggested for the glacial–interglacial monsoon circulation by Li et al. [50].

For short cold events, such as at times when polar and North Atlantic cold air surges burst, the westerlies are suddenly intensified and may shift south of the Tibet Plateau even in summer, causing a rapid expansion of the winter monsoon and a fast drop of the summer monsoon (Fig. 5b). But at times of the return of the North Atlantic heat supply pulse, the westerlies may suddenly weaken and shift some distance northwards or shift completely north of the plateau. This causes a rapid weak or full expansion of the summer monsoon, weathering the loess and weakly or moderately developing the soils (Fig. 5a). Thus, switching off of the thermohaline circulation and degree of heat supply in the North Atlantic substantially influences the strength of the summer monsoon through the westerlies. Obviously, these rapidly fluctuating short climatic events are superimposed on the long-term climatic changes of the Bond and orbital forcing cycles (Fig. 4).

In addition, the model provides a basis for understanding the large dust input rate associated with MIS 2/3 (Fig. 3). We think that the model's cold-trended feedback is an important part. This progressive intensification of the westerlies and the winter monsoon is synchronized with rapid cold surges in Heinrich events. This may destabilize the circulation system from a relatively stable warm climatic system to a stable cold system and generate the large-scale, high-frequency dust storms. Thus an extremely cold climate at the end of the feedback pathway could be expected. This could explain why very coarse size fraction events are found to lie at the ends of long-term (Bond) cooling cycles (Fig. 4).

Nevertheless, the model may not suit the Holocene short-term climatic change very well because there is no Laurentian ice sheet in the North Atlantic and the thermohaline circulation has never been switched off. Thus, the large monsoon changes of the Asian Holocene may suggest that the Asian monsoon system likely works at least in major part on its own during the Holocene.

Acknowledgements

We thank Prof. W. Dansgaard and Prof. J. Johnsen for providing GRIP ice core data and initial helpful comments. We are also grateful to Prof. S. Porter for his valuable suggestion to improve data processing and presentation and to Dr. D. Nettleton, Prof. Zhou Xiuji and Prof. Chen Longxun for their valuable comments on soils and climatic model. Many thanks are also due to Mr. Nu Lianqing, Mr. Yan Maodu, Mr. Zhao Zhijun and Mr. T. Sasaki for field work assistance and data manipulation. Helpful reviews were provided by G.C. Bond, N. Thouveny and an anonymous reviewer. This work is co-supported by grants from JSPS (Japan Society for the Promotion of Science), Ministry of Education of China (grant for Trans-Century Excellent Researchers and the Key Program), the National and CAS Tibet Research Project, and the INQUA 1997 Project. ***[RV]***

References

[1] L.X. Chen, East Asian Monsoon, Meteorology Press, Beijing, 1995, 250 pp.
[2] T.S. Liu, Loess and the Environment, China Ocean Press, Beijing, 1985, 251 pp.
[3] Z.S. An, T.S. Liu, Y.C. Lu, S. Porter, G.J. Kukla, X.H. Wu, Y.M. Hua, The long-term paleomonsoon variation recorded by the loess–paleosol sequence in central China, Quat. Int. 7/8 (1990) 91–95.
[4] S.C. Porter, Z. An, Correlation between climate events in the North Atlantic and China during the last glaciation, Nature 375 (1995) 305–308.
[5] H. Heinrich, Origin and consequences of cyclic ice rafting in the Northeast Atlantic Ocean during the past 130,000 years, Quat. Res. 29 (1988) 142–152.
[6] W.S. Broecker, Massive iceberg discharges as triggers for global climate change, Nature 372 (1994) 421–424.
[7] G.C. Bond, R. Lotti, Iceberg discharges into the North Atlantic on millennial time scales during the last glaciation, Science 267 (1995) 1005–1010.
[8] W. Dansgaard, S.J. Johnsen, H.B. Clausen, D. Dahi-Jensen, N.S. Gundestrup, C.U. Hammer, C.S. Hvidberg, J.P. Steffensen, A.E. Sveinbjornsdottir, J. Jouzel, G. Bond, Evidence for general instability of past climate from a 250-kyr ice-core record, Nature 364 (1993) 218–220.
[9] G. Bond, W. Broecker, S. Johnsen, J. McManus, L. Labeyrie, J. Jouzel, G. Bonani, Correlations between climate records from North Atlantic sediments and Greenland ice, Nature 365 (1993) 143–147.
[10] F. Sirocko, D. Grabe-Schonberg, A. McIntyre, B. Molfino, Teleconnections between the subtropical monsoon and

high-latitude climates during the last deglaciation, Science 272 (1996) 526–529.
[11] H. Fukusawa, I. Koizumi, Deep sea sediments in Japan Sea recording the late climatic changes in Asia (in Japanese with English abstr.), Chikyu Monthly 16 (1994) 678–684.
[12] D.W. Burbank, J.-J. Li, Age and palaeoclimatic significance of the loess of Lanzhou, north China, Nature 316 (1985) 429–431.
[13] J.-J. Li, J.-J. Zhu, J.-C. Kuang, F.-H. Chen, X.-M. Fang, D.-F. Mu, J.-X. Cao, L.-Y. Tang, T. Zhang, B.-T. Pan, Comparison of Lanzhou loess section of last glacial epoch with Antarctic Vostok ice core, Sci. China B 10 (1990) 1086–1094.
[14] Li, J.-J. et al., Uplift of Qinghai-Xizang (Tibet) Plateau and Global Change, Lanzhou University Press, Lanzhou, 1995, 210 pp.
[15] X.-M. Fang, J.-J. Li, E. Derbyshire, E.A. FitzPatrick, R.A. Kemp, Micromorphology of the Beiyuan loess–paleosol sequence in Gansu Province, China: geomorphological and paleoenvironmental significance, Palaeogeogr., Palaeoclimatol., Palaeoecol. 111 (1994) 289–303.
[16] X.-M. Fang, X.-R. Dai, J.-J. Li, J.-X. Cao, D.-H. Guang, Y.-P. Hao, J.-L. Wang, J.-M. Wang, Abruptness and instability of Asian monsoon — an example from soil genesis during the last interglacial, Sci. China B 26 (2) (1995) 154–160.
[17] FAO–UNESCO, Soil Map of the World, Vol. 1, Rome, 1988, 188 pp.
[18] C.L. Bascomb, A calcimeter for routine use on soil samples, Chem. Ind. 45 (1961) 1826–1827.
[19] X.-M. Fang, J.-J. Li, R. Van der Voo, C.M. Niocaill, X.-R. Dai, R. Kemp, E. Derbyshire, J.-X. Cao, J.-M. Wang, G. Wang, A record of the Blake event during the last interglacial paleosol in the western Loess Plateau of China, Earth Planet. Sci. Lett. 146 (1997) 73–82.
[20] Z.Y. Zhu, The formation of river terraces and evolution of drainage system in the middle reaches of the Yellow River, (in Chinese with English abstr.), J. Geogr. 44 (1989) 441–452.
[21] J.-J. Li, X.-M. Fang, R. Van der Voo, J.-J. Zhu, C.M. Niocaill, Y. Ono, B.-T. Pan, W. Zhong, J.-L. Wang, T. Sasaki, Y.-T. Zhang, J.-X. Cao, S.-C. Kang, J.-M. Wang, Magnetostratigraphic dating of river terraces: rapid and intermittent incision by the Yellow River of the northeastern margin of the Tibet Plateau during the Quaternary, J. Geophys. Res. 102 (1997) 10121–10132.
[22] D.G. Martinson, N.G. Pisias, J.D. Hays, J. Imbrie, T.C. Moore Jr., N.J. Shackleton, Age dating and the orbital theory of the ice ages: development of a high-resolution 0 to 300,000-year chronostratigraphy, Quat. Res. 27 (1987) 1–29.
[23] S. Tsukamoto, Infrared stimulated luminescence (IRSL) dating of Chinese loess deposits, Abstr. Annu. Conf. Jpn. Geogr. Soc., Tokyo Metropolitan University, Tokyo, 1997.
[24] B.H. Lin, R.M. Li, Stable isotopic evidence for summer monsoon changes on the Chinese Loess Plateau during the last 800 ka, Chin. Sci. Bull. 37 (18) (1995) 1691–1693.
[25] M. Stuiver, P.J. Reimer, Extended ^{14}C data base and revised CALIB 3.0 ^{14}C age calibration program, Radiocarbon 35 (1) (1993) 215–230.
[26] E. Bard, B. Hamelin, R.G. Fairbanks, A. Zindler, Calibration of the ^{14}C timescale over the past 30,000 years using mass spectrometric U–Th ages from Barbados corals, Nature 345 (1990) 405–410.
[27] E. Bard, M. Arnold, R.G. Fairbanks, ^{230}Th and ^{14}C ages obtained by mass spectrometry on corals, Radiocarbon 35 (1) (1993) 191–199.
[28] B.A. Maher, R.M. Taylor, Formation of ultrafine-grained magnetite in soils, Nature 336 (1988) 368–370.
[29] S.K. Banerjee, C.P. Hunt, X.-M. Liu, Separation of local signals from the regional paleomonsoon record of the Chinese loess plateau: a rock-magnetic approach, Geophys. Res. Lett. 20 (9) (1993) 843–846.
[30] C.P. Hunt, S.K. Banerjee, J.M. Han, P.A. Solheid, E. Oches, W.W. Sun, T.S. Liu, Rock-magnetic proxies of climate change in the loess–palaeosol sequences of the western Loess Plateau of China, Geophys. J. Int. 123 (1995) 232–244.
[31] M. Torii, Rock-magnetic study of sediments: a brief review of bulk sample methods, in: T. Yukutake (Ed.), The Earth's Central Part: Its Structure and Dynamics, Terra Scientific Publishing Company, Tokyo, 1995, pp. 57–73.
[32] T. Mishima, M. Torii, H. Fukusawa, K. Ooi, Y. Ono, X.-M. Fang, B.-T. Pan, J.-J. Li, Rock magnetic study of Chinese loess from Shajinping, Lanzhou, China, Soc. Geomag. Earth, Planet. Space Sci. Fall Meeting Abstract, Sapporo, 1997, p. 13.
[33] E.A. FitzPatrick, Soils: Their Formation, Classification and Distribution, Longmans, London, 1980, 353 pp.
[34] Y. Xong, Q.K. Li, Soils of China, Science Press, Beijing, 1990, 720 pp.
[35] L.H. Gile, F.F. Peterson, R.B. Grossman, Morphological and genetic sequences of carbonate accumulation in desert soils, Soil Sci. 101 (5) (1966) 347–360.
[36] R.A. Kemp, The cause of redness in some buried and non-buried soils in eastern England, J. Soil Sci. 36 (1985) 329–334.
[37] S. Nagajima, The Change of Earth Color (in Japanese), Future Press, Tokyo, 1994, 292 pp.
[38] K. Oi, H. Fukusawa, S. Iwata, M. Torii, Last 2.4 Ma changes of monsoon and westerly activities in East Asia, detected by clay mineral composition in loess–paleosol sequences at the inland area of China and deep-sea sediments of the Japan Sea (in Japanese with English abstr.), J. Geogr. 106 (1997) 249–259.
[39] G. Bond, W. Showers, M. Cheseby, R. Lotti, P. Almasi, P. deMenocal, P. Priore, H. Cullen, I. Hajdas, G. Bonani, A pervasive millennial-scale cycle in North Atlantic Holocene and glacial climates, Science 278 (1997) 1257–1266.
[40] Y.F. Shi (Ed.), The Chinese Holocene (in Chinese with English abstract), Science Press, Beijing, 1995, 257 pp.
[41] E.C. Grimm, G.L. Jacobson Jr., W.A. Watts, B.C.S. Hansen, K.A. Maasch, A 50,000-year record of climate oscillations

from Florida and its temporal correlation with the Heinrich events, Science 261 (1993) 198–200.
[42] N. Thouveny, J.L. de Beaulleu, E. Bonifay, K.M. Creer, J. Guiot, M. Icole, S. Johnsen, J. Jouzel, M. Reille, T. Williams, D. Williamson, Climate variations in Europe over the past 140 kyr deduced from rock magnetism, Nature 371 (1994) 503–506.
[43] R.C. Thunell, P.G. Mortyn, Glacial climate instability in the Northeast Pacific-ocean, Nature 376 (1995) 504–506.
[44] R. Thunell, D. Anderson, D. Gellar, Q.M. Miao, Sea-surface temperature estimates for the tropical western pacific during the last glaciation and their implications for the pacific warm pool, Quat. Res. 41 (1994) 255–264.
[45] B.K. Linsley, Oxygen-isotope record of sea level and climate variations in the Sulu Sea over the past 150,000 years, Nature 380 (1996) 234–237.
[46] D.Z. Yie, Y.X. Gao, Meteorology of the Tibet Plateau (in Chinese), Science Press, Beijing, 1988, 420 pp.
[47] W.F. Ruddiman, J.E. Kutzbach, Forcing of late Cenozoic Northern Hemisphere climate by plateau uplift in Southern Asia and the American West, J. Geophys. Res. 94 (D15) (1989) 18409–18427.
[48] J.E. Kutzbach, P.J. Guetter, W.F. Ruddiman, W.L. Prell, Sensitivity of climate to late Cenozoic uplift in Southern Asia and the American West: numerical experiments, J. Geophys. Res. 94 (D15) (1989) 18393–18407.
[49] M.C. Tang, E.R. Reiter, Plateau monsoons of the Northern Hemisphere: a comparison between North America and Tibet, Mon. Weather Rev. 112 (1984) 617–637.
[50] J.-J. Li, Z.-D. Feng, L.-Y. Tang, Later Quaternary monsoon pattern on the Loess Plateau of China, Earth Surf. Process. Landf. 13 (1988) 125–135.